

Multistate and multihypothesis discrimination with open quantum systems

Alexander Holm Kiilerich* and Klaus Mølmer†

Department of Physics and Astronomy, Aarhus University, Ny Munkegade 120, 8000 Aarhus C, Denmark



(Received 9 February 2018; published 14 May 2018)

We show how an upper bound for the ability to discriminate any number N of candidates for the Hamiltonian governing the evolution of an open quantum system may be calculated by numerically efficient means. Our method applies an effective master-equation analysis to evaluate the pairwise overlaps between candidate full states of the system and its environment pertaining to the Hamiltonians. These overlaps are then used to construct an N -dimensional representation of the states. The optimal positive-operator valued measure (POVM) and the corresponding probability of assigning a false hypothesis may subsequently be evaluated by phrasing optimal discrimination of multiple nonorthogonal quantum states as a semidefinite programming problem. We provide three realistic examples of multihypothesis testing with open quantum systems.

DOI: [10.1103/PhysRevA.97.052113](https://doi.org/10.1103/PhysRevA.97.052113)

I. INTRODUCTION

Quantum metrology is concerned with the discrimination of quantum states, Fig. 1(a), often with the purpose of distinguishing between different physical parameters governing the preparation or evolution of a quantum system [1]. In Hamiltonian parameter estimation a continuum of candidate parameter values are filtered by their different action on the state of a quantum probe while hypothesis testing considers scenarios with a discrete set of hypotheses $m = 1, 2, \dots, N$, for the Hamiltonian acting on the probe. In both cases, our ability to determine the true candidate hypothesis or physical parameter is ultimately limited by our ability to discern the corresponding signals obtained by measurements on the probe system.

In the present work we are interested in experiments with an open probe system whose interaction with a broadband environment validates the Born-Markov approximation. If the environment is left unmonitored, the interaction leads to decoherence of the system and to a loss of distinguishability, while a combined measurement on the probe system and its environment may yield much more information about the physical parameters governing the dynamics; see Fig. 1(b). Assuming that such a measurement is implementable, the ultimate precision is concerned not with the discrimination of reduced density-matrix candidates $\{\rho_m\}_{m=1}^N$ for the small system but rather with the discrimination of the, possibly, pure quantum states of the system and its environment $\{|\psi_m^{\text{SE}}\rangle\}_{m=1}^N$.

In this article we show how discrimination between an arbitrary number of (nonorthogonal) states of a quantum system may be employed to determine an upper bound for our ability to distinguish among different hypotheses concerning the evolution of a Markovian open quantum system. The full states of a system and a Markovian environment occupy in general a very large Hilbert space and the candidate states

of the combined system and their overlaps $\langle\psi_n^{\text{SE}}|\psi_m^{\text{SE}}\rangle$ are at a first glance intractable. Yet, it was shown in Ref. [2] how $\langle\psi_n^{\text{SE}}|\psi_m^{\text{SE}}\rangle$ can be calculated efficiently by propagating a so-called two-sided master equation for an effective density matrix which lives in the much smaller Hilbert space of the system alone.

For two candidate states $|\psi_1\rangle$ and $|\psi_2\rangle$ prepared with prior probabilities P_1 and P_2 , Helstrom derived in 1969 a general expression for the minimum error probability in discriminating them by a single measurement [3],

$$Q_e^{(\text{Helstrom})} = \frac{1}{2}(1 - \sqrt{1 - 4P_1P_2|\langle\psi_1|\psi_2\rangle|^2}). \quad (1)$$

Recent works, e.g., Refs. [4,5], have made progress towards deriving a general framework for cases with multiple hypotheses, but no closed-form expression has been found except in cases where the candidate density operators commute [6]. As pointed out by Helstrom [3] it is, however, clear that even for multiple hypotheses the error probability Q_e depends only on the pairwise overlaps between the candidate states and their prior probabilities.

Our presentation is structured as follows. In Sec. II we outline how the error probability in discriminating N arbitrary quantum states can be phrased as a semidefinite-programming problem for which numerically efficient algorithms exist. In Sec. III we rederive the main results of Ref. [2] for evaluating $\langle\psi_n^{\text{SE}}|\psi_m^{\text{SE}}\rangle$, and we show how the pairwise state overlaps among N candidate states can be applied to embed these states in a reduced Hilbert space of dimension N . Distinguishing N hypotheses for the evolution of the open quantum system is equivalent to a multistate discrimination problem on this Hilbert space. In Sec. IV we illustrate our theory by presenting three examples: (i) discriminating four candidates for the relative phase of a Rabi drive on an open two-level system, (ii) discriminating whether a low- Q cavity is coupled to 1, 2, 3, or 4 atoms, and (iii) using a sensor ion to determine the position of a nearby qubit ion in a doped crystal lattice structure. Finally, in Sec. V we conclude and provide an outlook.

*kiilerich@phys.au.dk

†moelmer@phys.au.dk

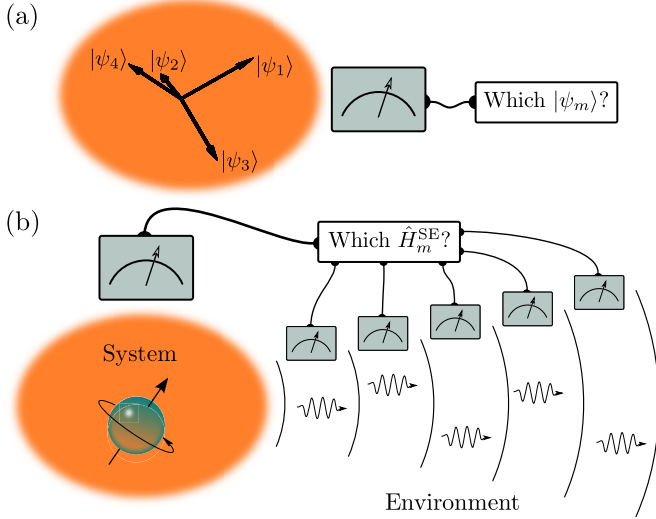


FIG. 1. (a) In state discrimination, a measurement is performed to distinguish between a set of N candidate states $\{|\psi_m\rangle\}_{m=1}^N$. (b) In hypothesis discrimination with an open quantum probe, a combined measurement on the system and its environment is performed to determine the true candidate from a set of N possible Hamiltonians $\{\hat{H}_m^{SE}\}_{m=1}^N$ of the system or the combined system and environment.

II. OPTIMAL STATE DISCRIMINATION

One may specify different goals and hence measures of the quality of a state discrimination process, depending on the number of copies of the quantum system available [7] and depending on the cost and reward for making wrong and correct estimates [8]. In the limit where measurements on asymptotically many copies M of the quantum probe system are available, the probability of making an erroneous assignment decreases exponentially with M . The exponent obeys the quantum Chernoff bound [9], which was recently generalized to cases with multiple candidate states [10].

In the present study we are interested in the information obtainable by performing a measurement on a single quantum system. We assume that the system is prepared with probability P_m in one of N different, mixed quantum states $\{\rho_m\}_{m=1}^N$, and that we can perform measurements on the system with outcomes that we combine into our assignment $\lambda = 1, 2, \dots, N$ of the most likely state. We quantify a given measurement strategy by the *error probability* of assigning a false state (hypothesis) based on the outcome λ of a measurement performed on the system,

$$Q_e = \sum_{m=1}^N P_m \sum_{\substack{n=1 \\ n \neq m}}^N P(\lambda = n | \rho_m). \quad (2)$$

To be able to assign N possible states, the measurement must have N possible outcomes, so for a Hilbert space of dimension $d < N$, we have recourse to generalized (nonprojective) measurements with fundamentally ambiguous outcomes. Such measurements are defined by a positive-operator valued measure (POVM) with effects $\{\hat{E}_m\}_{m=1}^N$ which are positive semidefinite ($\hat{E}_m \geq 0$) and sum to identity $\sum \hat{E}_m = \mathbb{I}$ [11]. The probability to obtain an outcome n if the *true* state is ρ_m

is then $P(\lambda = n | \rho_m) = \text{Tr}(\hat{E}_n \rho_m)$, so by applying $\sum \hat{E}_m = \mathbb{I}$ and $\sum P_m = 1$ we may rewrite Eq. (2),

$$Q_e(\{\hat{E}_m\}_{m=1}^N) = 1 - \sum_{m=1}^N P_m \text{Tr}(\hat{E}_m \rho_m). \quad (3)$$

The task of obtaining the optimal POVM, which minimizes the error probability for a given set of candidate states $\{\rho_m\}_{m=1}^N$ with (prior) probabilities $\{P_m\}_{m=1}^N$ defines a semidefinite programming problem [12]:

$$\begin{aligned} &\text{minimize} && Q_e(\{\hat{E}_m\}_{m=1}^N) \\ &\text{subject to} && \hat{E}_m \geq 0 \quad \forall m \in \{1, \dots, N\} \\ &\text{and} && \sum_{m=1}^N \hat{E}_m = \mathbb{I}. \end{aligned} \quad (4)$$

Recent studies provide analytic solutions for this problem in the case of discriminating three qubit states ($N = 3$, $d = 2$) [4] with arbitrary prior probabilities or any number of *a priori* equally probable qubit states [13]. Furthermore, it was recently realized that any N -outcome measurement can be decomposed into sequences of nested two-outcome measurements which allow straightforward numerical optimization [5]. A detailed discussion of the state discrimination problem as a convex optimization task and a general solution by semidefinite programming was provided in Ref. [14]. In the present study we apply the CVX package for specifying and solving convex programs in Matlab [15,16].

III. HYPOTHESIS TESTING WITH OPEN QUANTUM SYSTEMS

Hypothesis testing is the task of discriminating the evolution of a probe system subject to one of a discrete set of candidate Hamiltonians. To distinguish different hypotheses, a system may be subject to continuous monitoring by a probe beam or information may be obtained by, e.g., homodyne detection or photon counting of the radiation emitted by the system [17–19]. A variety of studies on such strategies point out that temporal correlations in the transmitted or emission signals are essential for their achievable precision [20–29].

As argued in [2,30,31], the Markovian nature of the system-environment interaction implies that the discernibility of the (unmeasured) quantum states of the system and environment provides a theoretical upper bound for our practical ability to distinguish the different hypotheses by, e.g., continuous monitoring of the environment degrees of freedom [28,29]. Each individual hypothesis m thus leads to a particular unmeasured quantum state $|\psi_m^{SE}\rangle$ of the system and the environment at a given time t and hypothesis testing is equivalent to the problem of discriminating the states $\{|\psi_m^{SE}(t)\rangle\}_{m=1}^N$. Due to the large Hilbert space dimension of the environment, these states are generally not accessible. Nevertheless, following the idea of Ref. [2], we show in this section that in situations where the Born-Markov approximation applies to the system-environment interaction, the overlaps between any two candidate states can be evaluated by solving a two-sided master equation for an effective density operator on the small system Hilbert space alone. We subsequently show how the

overlaps between all pairs of states can be used to construct a low-dimensional representation of the problem to which the technique (4) of Sec. II applies.

A. Two-sided master equation for the state overlaps

The distinct hypotheses can be formally mapped to the states $|m\rangle$ of an N -level ancillary system such that the evolution of the system and environment is conditioned on the state of the ancilla via the Hamiltonian

$$\hat{H}^{\text{ASE}} = \sum_{m=1}^N |m\rangle \langle m| \otimes \hat{H}_m^{\text{SE}}, \quad (5)$$

where the candidates $\hat{H}_m^{\text{SE}}(t) = \hat{H}_m + \hat{V}_m^{\text{SE}}$ for the system-environment Hamiltonian in the interaction picture may be separated into candidates for the part acting on the system alone \hat{H}_m and candidates \hat{V}_m^{SE} for the system-environment interaction.

While the ancilla, system, and environment are initially prepared in a separable pure state $\frac{1}{\sqrt{N}} \sum_{m=1}^N |m\rangle \otimes |\psi^{\text{SE}}(t=0)\rangle$, evolution under the Hamiltonian (5) yields, after a time t , an entangled state,

$$|\psi(t)\rangle = \frac{1}{\sqrt{N}} \sum_{m=1}^N |m\rangle \otimes |\psi_m^{\text{SE}}(t)\rangle. \quad (6)$$

Instead of the explicit separation in ancilla (A) and system-environment (SE) components in Eq. (6), we shall separate the complete system in ancilla-system (AS) and environment degrees of freedom. Assuming a weak coupling to a memoryless environment, the state ρ^{AS} of the ancilla-system obeys a Born-Markov master equation in the interaction frame [$\hbar = 1$],

$$\begin{aligned} \dot{\rho}^{\text{AS}} = & -i[\hat{H}^{\text{AS}}, \rho^{\text{AS}}] - \int_0^\infty dt' \text{Tr}_E([\hat{V}^{\text{ASE}}(t), [\hat{V}^{\text{ASE}}(t'), \\ & \times \rho^{\text{AS}}(t') \otimes \rho^{\text{E}}(0)]]). \end{aligned} \quad (7)$$

In Eq. (7), the unitary part of the evolution is governed by a Hamiltonian

$$\hat{H}^{\text{AS}} = \sum_{m=1}^N |m\rangle \langle m| \otimes \hat{H}_m, \quad (8)$$

and the interaction with the environment described by

$$\hat{V}^{\text{ASE}}(t) = \sum_{m=1}^N |m\rangle \langle m| \otimes \hat{V}_m^{\text{SE}}(t). \quad (9)$$

The ancilla-system state can be put on the form of a block matrix,

$$\rho^{\text{AS}}(t) = \frac{1}{N} \sum_{n,m=1}^N \rho_{nm}(t) |n\rangle \langle m|, \quad (10)$$

where the operators $\rho_{nm}(t)$ on the system Hilbert space are all equal to the projection operator on the initial state of the system at time $t = 0$.

As seen from Eq. (6), the overlap between the n th and m th system-environment candidate states can be obtained as the

expectation value of $|n\rangle \langle m|$,

$$\begin{aligned} \langle \psi_n^{\text{SE}} | \psi_m^{\text{SE}} \rangle &= N \langle \psi(t) | n \rangle \langle m | \psi(t) \rangle \\ &= N \text{Tr}_{\text{AS}}[|n\rangle \langle m| \rho^{\text{AS}}(t)] \\ &= \text{Tr}_S[\rho_{mn}(t)]. \end{aligned} \quad (11)$$

Inserting Eq. (10) as an ansatz into Eq. (7) produces a set of equations,

$$\begin{aligned} \dot{\rho}_{nm} = & -i(\hat{H}_n \rho_{nm} - \rho_{nm} \hat{H}_m) \\ & - \int_0^\infty dt' \text{Tr}_E(\hat{V}_n^{\text{SE}}(t) \hat{V}_n^{\text{SE}}(t') \rho_{nm}(t) \otimes \rho^{\text{E}}(0) \\ & + \rho_{nm}(t) \otimes \rho^{\text{E}}(0) \hat{V}_m^{\text{SE}}(t') \hat{V}_m^{\text{SE}}(t) \\ & - \hat{V}_n^{\text{SE}}(t) \rho_{nm}(t) \otimes \rho^{\text{E}}(0) \hat{V}_m^{\text{SE}}(t') \\ & - \hat{V}_n^{\text{SE}}(t') \rho_{nm}(t) \otimes \rho^{\text{E}}(0) \hat{V}_m^{\text{SE}}(t)). \end{aligned} \quad (12)$$

We refer to these as *two-sided* master equations because the matrix argument $\rho_{nm}(t)$ is acted upon by the different candidate Hamiltonians from the left- and right-hand sides.

Suppose now that, in the rotating-wave approximation, the system-environment interaction can be written on a Jaynes-Cummings form,

$$\hat{V}_m^{\text{SE}} = \sum_k (g_m^{(k)} \hat{a}_k \hat{S}_m^\dagger e^{-i\delta_k t} + (g_m^{(k)})^* \hat{a}_k^\dagger \hat{S}_m e^{i\delta_k t}), \quad (13)$$

where the sum runs over the bosonic bath modes with annihilation (creation) operators \hat{a}_k (\hat{a}_k^\dagger), detuned by δ_k from the system resonance. Hypotheses for the interaction with the environment are represented by the system operators \hat{S}_m and complex coupling coefficients $g_m^{(k)} = |g_m^{(k)}| e^{i\phi_m^{(k)}}$ to the individual modes.

If we assume the environment to be in the vacuum state $\rho^{\text{E}}(0) = \sum_k |0_k\rangle \langle 0_k|$, performing the partial trace over the environment in Eq. (12) yields a two-sided master equation,

$$\begin{aligned} \dot{\rho}_{nm} = & -i(\hat{H}_n \rho_{nm} - \rho_{nm} \hat{H}_m) \\ & + \hat{c}_n \rho_{nm}(t) \hat{c}_m^\dagger - \frac{1}{2}(\hat{c}_n^\dagger \hat{c}_n \rho_{nm} - \rho_{nm} \hat{c}_m^\dagger \hat{c}_m), \end{aligned} \quad (14)$$

where the candidate dissipation operators are defined as $\hat{c}_m = \sqrt{\gamma_m} \hat{S}_m e^{-i\phi_m}$. Here the damping rates γ_m and phases ϕ_m are obtained from the integrated correlation functions of the environment,

$$\Gamma_{ab}(t) = \int_0^\infty dt' \sum_k (g_a^{(k)})^* g_b^{(k)} e^{-i\delta_k(t-t')}. \quad (15)$$

Consistent with Fermi's golden rule, due to the time integral, one obtains $\Gamma_{ab}(t) = 2\pi (g_a^{(k_s)})^* g_b^{(k_s)}$ with $\delta_{k_s} = 0$, such that $\gamma_m = 2\pi |g_m^{(k_s)}|^2$ and $\phi_m = \phi_m^{(k_s)}$. Note that, for simplicity, we included only a single environment and a single transition operator. In the case of hypotheses concerning multiple environmental couplings, a corresponding sum over dissipation operators, $\hat{c}_m \rightarrow \{\hat{c}_{j,m}\}_{j=1}^J$, is employed in the master equation (14).

The solution of the uncoupled equations (14) yields by Eq. (11) the temporal dynamics of the overlap between any pair of the *full* states of the system and environment pertaining to the different hypotheses for the effective system Hamiltonians \hat{H}_m and relaxation operators \hat{c}_m . Hence the numerically intractable

problem of evolving the full states in the very large system and environment Hilbert space is reduced to the much simpler task of evolving $(N^2 - N)/2$ matrices with the dimension of the smaller probe system.

B. Low-dimensional representation of states of the system and its environment

Although the full state of a system and its environment lives in a formally infinite-dimensional Hilbert space, the discrete nature of the hypothesis testing problem implies that at any time we have at most N different possible states to distinguish. These span a (time-dependent) subspace of dimension N which is sufficient to fully characterize the discrimination problem. To apply the semidefinite programming methods of Sec. II, let us define an orthogonal basis $\{|\phi_n\rangle\}_{n=1}^N$ for this subspace such that each candidate state can be expressed as a linear combination,

$$|\psi_m^{\text{SE}}\rangle = \sum_{n=1}^m C_n^{(m)} |\phi_n\rangle,$$

where the $C_n^{(m)}$ are complex expansion coefficients.

We shall now outline how one may in general define a basis and obtain the $C_n^{(m)}$: let the first basis state be the first candidate state $|\phi_1\rangle = |\psi_1\rangle$, i.e., $C_n^{(1)} = \delta_{n1}$. The second state is then used to define the second basis state, $\text{span}(|\psi_1^{\text{SE}}\rangle, |\psi_2^{\text{SE}}\rangle) = \text{span}(|\phi_1\rangle, |\phi_2\rangle)$, such that $C_n^{(2)} = 0$ for $n > 2$. Since any of the basis states may be multiplied by an arbitrary complex phase factor, we may further use the convention that $C_2^{(2)}$ is positive which together with the overlap $\langle\psi_1^{\text{SE}}|\psi_2^{\text{SE}}\rangle$ and the normalization criterion completely determines $|\phi_2\rangle$. Similarly the third candidate defines the third basis state and we set $C_3^{(3)} \in \mathbb{R}_{\geq 0}$. By continuing in this manner, we represent the states of the system and the environment as a sequence of N -dimensional vectors

$$\begin{matrix} \mathbf{C}^{(1)} & \mathbf{C}^{(2)} & \mathbf{C}^{(3)} & \dots & \mathbf{C}^{(N)} \\ \parallel & \parallel & \parallel & & \parallel \\ \begin{pmatrix} 1 \\ 0 \\ \vdots \\ 0 \end{pmatrix} & \begin{pmatrix} C_1^{(2)} \\ C_2^{(2)} \\ 0 \\ \vdots \\ 0 \end{pmatrix} & \begin{pmatrix} C_1^{(3)} \\ C_2^{(3)} \\ C_3^{(3)} \\ 0 \\ \vdots \\ 0 \end{pmatrix} & \dots & \begin{pmatrix} C_1^{(N)} \\ C_2^{(N)} \\ \vdots \\ C_N^{(N)} \end{pmatrix} \end{matrix}, \quad (16)$$

where all state amplitudes are given by a recursive procedure:

$$C_n^{(m)} = \frac{1}{C_n^{(n)}} \left(\langle\psi_n|\psi_m\rangle - \sum_{k=1}^{n-1} C_k^{(n)*} C_k^{(m)} \right) \quad (17)$$

for $1 \leq n \leq m-1$ and

$$C_m^{(m)} = \sqrt{1 - \sum_{k=1}^{m-1} |C_k^{(m)}|^2}. \quad (18)$$

It may in a given hypothesis testing scenario occur that two or several candidate states become identical. The number of POVM elements is then reduced and for some outcomes

of our protocol we have recourse to select the one of the corresponding hypotheses with the largest prior probability.

IV. EXAMPLES

The ideas and methods presented in Secs. II and III allow us to evaluate the minimum error probability in the assignment of one of *any* number of distinct hypotheses for the evolution of an open quantum system as a function of the duration t of an experiment. Here we provide three examples which illustrate different aspects of our theory and its application.

A. Phase of a Rabi drive

We first examine a two-level system driven resonantly with a known Rabi frequency Ω but with an unknown complex phase ϕ_m . In a frame rotating with the resonance frequency, the candidate Hamiltonians can be written as

$$\hat{H}_m = \Omega[\cos(\phi_m)\hat{\sigma}_x + \sin(\phi_m)\hat{\sigma}_y]/2. \quad (19)$$

In this example we consider the phases $\phi_m = \pi(m-1)/2$ as illustrated in the inset of Fig. 2, and we assume that the atomic excitation decays into the environment at a known rate γ such that $\hat{c} = \sqrt{\gamma}\hat{\sigma}_-$. The Rayleigh component of the emitted radiation is in phase with the driving field and homodyne detection should thus gradually reveal the value of ϕ_m . In contrast, photon counting tracks the intensity of the emitted radiation and hence maps the excitation of the system which is independent of ϕ_m .

The full curve in Fig. 2 shows the minimum error probability $Q_e(t)$ calculated from our theory as a function of the duration t of the experiment. Initially $Q_e(t=0) = 75\%$, reflecting that each of the four hypotheses are *a priori* equally probable ($P_m = 1/4$), while for large times they may be unambiguously discriminated. Interestingly, however, $Q_e(t)$ is not a monotonous

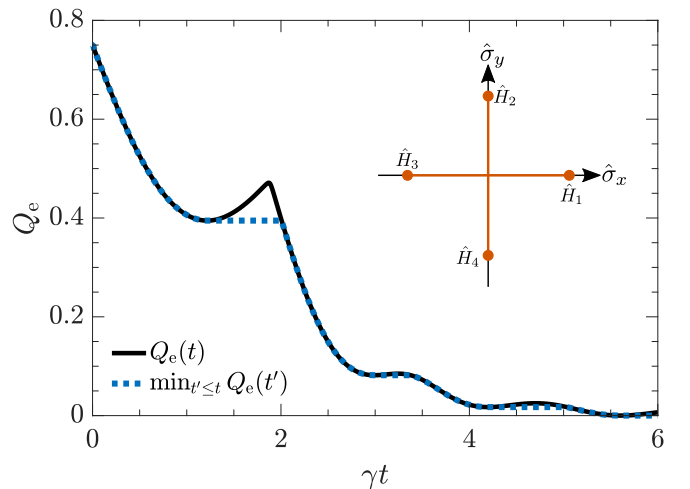


FIG. 2. Phase of a Rabi drive on a two-level system Eq. (19) is determined by performing a combined measurement on the atom and the emitted field. Inset: the four hypotheses are $\hat{H}_1 = \Omega\hat{\sigma}_x/2$, $\hat{H}_2 = \Omega\hat{\sigma}_y/2$, $\hat{H}_3 = -\Omega\hat{\sigma}_x/2$, and $\hat{H}_4 = -\Omega\hat{\sigma}_y/2$. Main figure: the probability of assigning a wrong hypothesis is shown for $\Omega = 2\gamma$ and an atom initialized in its ground state. The dotted curve shows the smallest error probability reachable by any given time t .

function of t . For instance, it reaches a minimum around $\gamma t \simeq 1.25$ and if for some reason the experiment lasts a little longer, $\gamma t \lesssim 2$, the ability to discriminate the four cases deteriorates. The reason is that, irrespective of the excitation phase, the atomic Bloch vector approaches the vertical direction around $\Omega t \simeq \pi$, and only the emitted radiation provides any information until the Bloch vector candidates evolve further. It is thus sometimes favorable to perform a measurement on the atom and the field at an earlier time and keep the result rather than wait for more data to accumulate. The dotted curves track the minimum error probability obtainable by performing a measurement before any given time t and hence represent the lowest error achievable in an experiment of duration t .

B. Number of atoms inside a cavity

Here we imagine a cavity field driven by a (classical) field of strength u and interacting with an unknown but small number of atoms. Due to an outcoupling at a rate κ from the cavity, the emitted radiation from the spins can be monitored and we further assume that the experimental setup allows direct measurements on the atomic ensemble. The atoms are modeled as N two-level systems of which m are coupled linearly with strength g to a single cavity mode and $N - m$ are uncoupled. Assuming the bad cavity limit, the field may be adiabatically eliminated leading to an effective Hamiltonian and relaxation of the atoms. The different hypotheses concerning the number of spins inside the cavity are hence characterized by N sets of Hamiltonians and relaxation operators,

$$\begin{aligned}\hat{H}_m &= g(\alpha \hat{S}_+^{(m)} + \alpha^* \hat{S}_-^{(m)}), \\ \hat{c}_m &= \sqrt{\gamma_p} \hat{S}_-^{(m)},\end{aligned}\quad (20)$$

where $\hat{S}_\pm^{(m)} = \sum_{i=1}^m \hat{\sigma}_\pm^{(i)}$, $\alpha = 2u/\kappa$, and $\gamma_p = 4g^2/\kappa$ is the Purcell-enhanced decay rate. We assume that the number of atoms coupled to the cavity is Poisson distributed with mean value $\mu = 1.5$. The probabilities prior to the experiment are hence $P_m \propto \mu^m/m!$.

Figure 3 shows the evolution of the minimum error probability in distinguishing the cases of $m = 1, 2, 3$, and 4 atoms inside the cavity. Results are shown for a weakly, a moderately, and a strongly driven cavity, respectively. While it is never favorable to drive the cavity very weakly since this does not lead to a fluorescence signal with much structure, it is evident that the moderate driving case outperforms the strong driving case for a brief period around $\gamma_p t \simeq 2.5$. However, the dotted curves, tracking the minimum error probability obtainable by performing a measurement at an optimal time before t , shows that the stronger driving is always favorable.

C. Relative positions of a dopant ion

Our final example concerns testing of the relative positions between two impurity dipoles in a lattice structure. Rare-earth-ion dopants in inorganic crystals have permanent electric dipole moments which are different depending on whether each ion is excited or not and may hence be used for controlled gates in a quantum computation [33,34]. Such systems are produced by low random doping during crystal growth and, for applications in a quantum sensor or computer, one may want

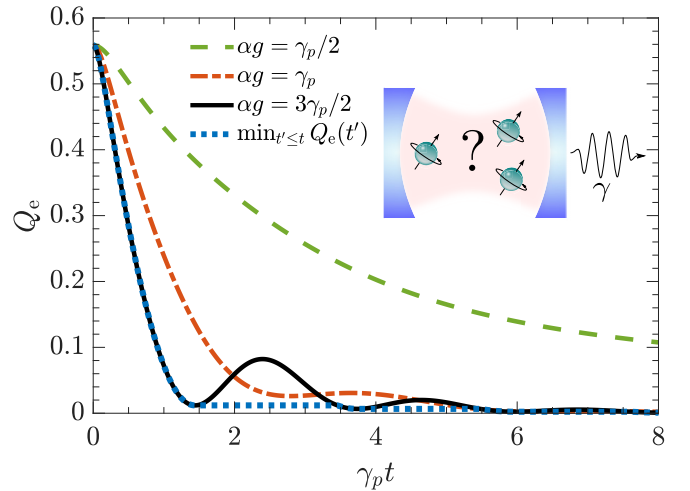


FIG. 3. Inset: an unknown number of atoms are coupled to a driven cavity. The number is estimated by performing a combined measurement on the atomic spins and the field emitted from the cavity. The hypotheses are $m = 1, 2, 3$, and 4 atoms and the system evolves according to the Hamiltonian (20). Main figure: the probability of assigning a false hypothesis is shown for weak driving $\alpha g = \gamma_p/2$, for moderate driving $\alpha g = \gamma_p$, and for strong driving $\alpha g = 3\gamma_p/2$. The dotted curve shows the smallest error probability reached before any given time t for the underdamped cases where local minima occur in $Q_e(t)$.

to assess the relative positions of the individual ions (qubits) by probing their interactions. A generic version of this kind of setup in a cubic lattice structure with lattice constant a is illustrated in Fig. 4(a). We assume dilute doping such that a read-out (sensor) ion couples only to a single qubit ion and we introduce a simple model of each ion as a two-level system. We let the sensor ion relax radiatively at a rate γ and assume the qubit ion states to be long lived. To obtain a fluorescence signal, the sensor is driven by a laser field with Rabi frequency Ω_s and detuned by δ_s from the bare transition frequency. We assume also the possibility to resonantly drive the qubit ion with a Rabi frequency Ω_q in order to optimize the sensing capabilities. The candidate Hamiltonians may hence be written

$$\begin{aligned}\hat{H}_m &= \frac{\Omega_s}{2} \hat{\sigma}_x^{(s)} + \frac{\Omega_q}{2} \hat{\sigma}_x^{(q)} - \delta_s |e_s\rangle \langle e_s| \\ &\quad + \Delta_m |e_q\rangle \langle e_q| \otimes |e_s\rangle \langle e_s|,\end{aligned}\quad (21)$$

where the latter term accounts for the state-dependent shift in frequency of the sensor ion due to the dipole-dipole interaction with the qubit ion [35],

$$\Delta_m = \left(\frac{\epsilon + 2}{3\epsilon} \right)^2 \frac{\mu_s \mu_q}{4\pi\epsilon_0 r_m^3} [\hat{\mu}_s \cdot \hat{\mu}_q - 3(\hat{\mu}_s \cdot \hat{r}_m)(\hat{\mu}_q \cdot \hat{r}_m)].\quad (22)$$

Here $\mu_{s(q)} = \mu_{s(q)} \hat{\mu}_{s(q)}$ is the difference in permanent electric dipole moment between the excited and ground state of the sensor (qubit) ion and $\mathbf{r}_m = r_m \hat{r}_m$ is the vector between the sensor and the qubit with which the hypothesis testing is concerned. The prefactor, where ϵ is the relative permittivity at zero frequency, accounts for local field corrections due to the crystal host material. One example is Eu^{3+} or Pr^{3+} ions

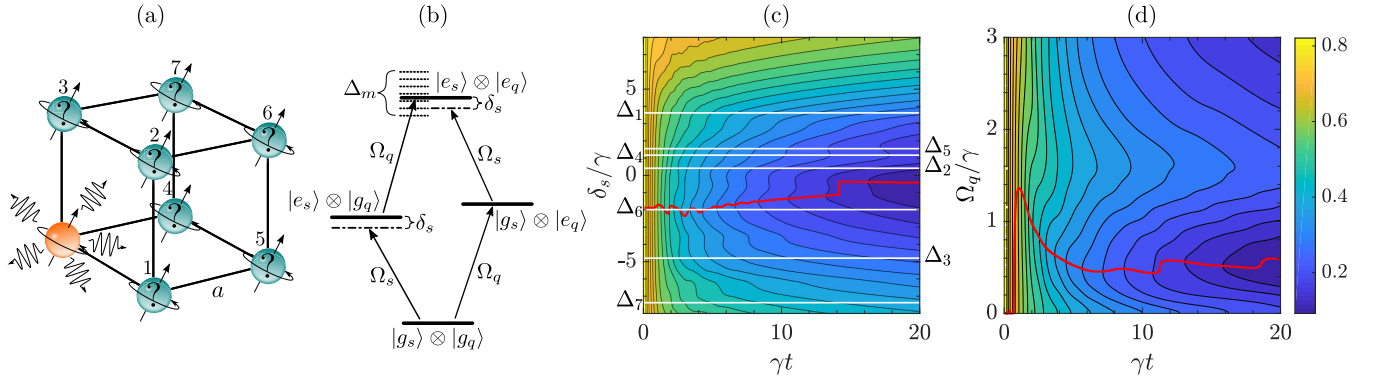


FIG. 4. (a) Position of a qubit ion (green spin) in a cubic lattice structure with lattice constant a affects the fluorescence signal emitted by a sensor ion (orange spin) of a different species at a nearby lattice position and the internal state of the two ions. In our example $\mu_s = \mu_q = (0.5, 0.3, 0.8)^T$ such that each of the seven possible marked positions yield a distinct energy shift of the sensor ion as given by Eq. (22). (b) The level structure of the Hamiltonian (21) of the two ions. The qubit ion is resonantly driven with a Rabi frequency Ω_q and the sensor ion is driven with a Rabi frequency Ω_s and a detuning δ_s from resonance. The sensor excited state is shifted by Δ_m due to the excited qubit ion. (c) Contour plot showing the probability Q_e of assigning a wrong lattice position to the qubit ion as a function of time and the (constant) detuning δ_s of the sensor ion drive. The red line tracks the constant value of δ_s which minimizes $Q_e(t)$ at any given time. The white lines mark the energy shifts Δ_m/γ associated with each of the seven possible positions in (a). (d) Contour plot showing the probability Q_e of assigning a wrong lattice position as a function of time and the (constant) strength of the qubit drive Ω_q with $\delta_s = 0$. The red line tracks the constant value of Ω_q which minimizes $Q_e(t)$ for any given probing time. Results in (c) and (d) are shown for $\Omega_s = 3\gamma$, $(\frac{\epsilon+2}{3\epsilon})^2 \frac{\mu_s \mu_q}{4\pi\epsilon_0} = 5\gamma a^3$, and equal priors $P_m = 1/7$.

doped in an YAlO_3 or an Y_2SiO_5 crystal [36]. A suitable sensor ion could be Ce^{3+} , which has a large difference μ_s in static dipole moment [37]. A level diagram for the Hamiltonian (21) is shown in Fig. 4(b) and the level shift as well as the driven transitions are indicated.

Imagine first that we prepare the qubit ion in the excited state and then turn off the qubit drive ($\Omega_q = 0$). As illustrated in Fig. 4(b) the resonance frequency of the excited state is then shifted by Δ_m in a manner depending on the position of the qubit ion. It is intuitively clear that a higher sensitivity can be obtained if the system is driven at the actual resonance, i.e., by detuning the sensor ion driving laser such that δ_s matches the true Δ_m . In Fig. 4(c), the contour plot shows the error probability as a function of time and the (constant) value of δ_s . The red curve tracks the optimum which is seen to be located near the mean value of the Δ_m . Based on this understanding, one could imagine an optimized scheme where δ_s is cycled through the different Δ_m candidates with an appropriate portion of the total experimental time allocated to each.

By preparing an excited qubit the last term in Eq. (21) remains fully active at all times while driving the qubit yields a transient evolution of the system which might depend more strongly on Δ_m . To investigate this, we show in Fig. 4(d) a contour plot of the error probability as a function of time and the qubit drive strength. The red line tracks the (constant) values of Ω_q which minimizes $Q_e(t)$ at any given time. Interestingly, for short times a relatively strong drive is favorable. This can be explained by the same mechanisms as in the previous example: when the system is strongly driven, it undergoes oscillations which are more pronounced at short times and whose frequency is modulated by Δ_m . For longer times it becomes favorable to maintain the excited state for longer durations and with the parameters used here the optimal value lies around $\Omega_q \simeq 0.5\gamma$.

We presented this example for dopant ions but the general idea may be relevant in a number of similar setups. For

example, the dipole-dipole potential between neutral atoms similarly yields an energy shift of the form Eq. (22) which is responsible for, e.g., the Rydberg blockade mechanism [38]. Hence our formalism could be fitted to the determination of the relative positions of Rydberg atoms in an optical lattice structure. Another platform is the sensing of a remote nuclear spin \hat{I} by an electron spin \hat{S} . Here the frequency shift is due to the hyperfine coupling [39–41]. For instance, the electron spin of an NV center can be used to sense the position of a ^{13}C impurity in a vapor deposited (CVD) diamond which has a ^{13}C abundance of less than 0.01% [42].

V. CONCLUSION AND OUTLOOK

We have evoked how optimal discrimination between an arbitrary number of quantum states may be phrased as a semidefinite programming problem for which efficient numerical solutions are available. We then utilize that distinguishing a set of N hypotheses for the evolution of a Markovian open quantum system is equivalent to the discrimination of a set of time-dependent states of the full system and its environment. We show how their overlaps may be calculated in a straightforward manner and used to construct a lower-dimensional representation which is suitable for numerical treatment. This allows us to evaluate a lower (quantum) bound to the probability of assigning a false hypothesis, and the three examples presented in this article serve to illustrate some insights that may be obtained by such an analysis.

For the example in Sec. IV C, we show how different but constant values of the qubit ion Rabi frequency and the detuning in the driving frequency of the sensor ion lead to different error probabilities. In optimal control, the bound could be further optimized by allowing time-dependent parameters $\Omega_q(t)$ and $\delta_s(t)$. More generally, by following this line of thought our formalism is suitable for systematic optimization of the sensing capabilities in a given quantum

setup by, e.g., controlling auxiliary Hamiltonian parameters or environmental coupling strengths.

Finally, we want to emphasize that our quantum bound may pertain to a highly nonlocal measurement performed on the full state of the system and its environment. Such a measurement is in general infeasible to implement and in real experimental situations one has recourse to perform a more conventional measurement of the environment. For instance, the radiation emitted by an open system may be monitored by photon counting or homodyne demodulation [20,21,23–27], and the signal possibly combined with a final projective measurement on the system. In Ref. [29] we compare the performance of such an approach to the quantum bound for dual hypothesis testing with a two-level open quantum system. Depending

on the setup, different monitoring schemes are favorable as discussed in relation to the example of Sec. IV A. See, e.g., Refs. [22,28] for further studies of hypothesis testing with continuous measurements.

ACKNOWLEDGMENTS

The authors would like to thank Frank Verstraete and Andreas Walther for helpful discussions and acknowledge financial support from the Villum Foundation and the European Union's Horizon 2020 research and innovation programme under Grant No. 712721 (NanOQTech). A.H.K. further acknowledges financial support from the Danish Ministry of Higher Education and Science.

-
- [1] V. Giovannetti, S. Lloyd, and L. Maccone, Quantum Metrology, *Phys. Rev. Lett.* **96**, 010401 (2006).
 - [2] K. Mølmer, Hypothesis Testing with Open Quantum Systems, *Phys. Rev. Lett.* **114**, 040401 (2015).
 - [3] C. W. Helstrom, Quantum detection and estimation theory, *J. Stat. Phys.* **1**, 231 (1969).
 - [4] D. Ha and Y. Kwon, Complete analysis for three-qubit mixed-state discrimination, *Phys. Rev. A* **87**, 062302 (2013).
 - [5] M. Rosati, G. De Palma, A. Mari, and V. Giovannetti, Optimal quantum state discrimination via nested binary measurements, *Phys. Rev. A* **95**, 042307 (2017).
 - [6] C. W. Helstrom, J. W. S. Liu, and J. P. Gordon, Quantum-mechanical communication theory, *Proc. IEEE* **58**, 1578 (1970).
 - [7] E. Davies, Information and quantum measurement, *IEEE Trans. Inf. Theory* **24**, 596 (1978).
 - [8] A. Peres and D. R. Terno, Optimal distinction between non-orthogonal quantum states, *J. Phys. A: Math. Gen.* **31**, 7105 (1998).
 - [9] K. M. R. Audenaert, J. Calsamiglia, R. Muñoz-Tapia, E. Bagan, Ll. Masanes, A. Acín, and F. Verstraete, Discriminating States: The Quantum Chernoff Bound, *Phys. Rev. Lett.* **98**, 160501 (2007).
 - [10] K. Li, Discriminating quantum states: The multiple Chernoff distance, *Ann. Stat.* **44**, 1661 (2016).
 - [11] H. M. Wiseman and G. J. Milburn, *Quantum Measurement and Control* (Cambridge University Press, Cambridge, UK, 2010).
 - [12] L. Vandenberghe and S. Boyd, Semidefinite programming, *SIAM Rev.* **38**, 49 (1996).
 - [13] J. Bae and W.-Y. Hwang, Minimum-error discrimination of qubit states: Methods, solutions, and properties, *Phys. Rev. A* **87**, 012334 (2013).
 - [14] Y. C. Eldar, A. Megretski, and G. C. Verghese, Designing optimal quantum detectors via semidefinite programming, *IEEE Trans. Inf. Theory* **49**, 1007 (2003).
 - [15] M. Grant and S. Boyd, CVX: Matlab software for disciplined convex programming, version 2.1, 2014, <http://cvxr.com/cvx>
 - [16] M. Grant and S. Boyd, Graph implementations for nonsmooth convex programs, in *Recent Advances in Learning and Control*, Lecture Notes in Control and Information Sciences, edited by V. Blondel, S. Boyd, and H. Kimura (Springer-Verlag Limited, Berlin, 2008), pp. 95–110, http://stanford.edu/boyd/graph_dcp.html
 - [17] K. W. Murch, S. J. Weber, C. Macklin, and I. Siddiqi, Observing single quantum trajectories of a superconducting quantum bit, *Nature (London)* **502**, 211 (2013).
 - [18] K. Jacobs, Feedback control for communication with non-orthogonal states, *Quantum Inf. Comput.* **7**, 127 (2007).
 - [19] D. Tan, N. Foroozani, M. Naghiloo, A. H. Kiilerich, K. Mølmer, and K. W. Murch, Homodyne monitoring of postselected decay, *Phys. Rev. A* **96**, 022104 (2017).
 - [20] H. Mabuchi, Dynamical identification of open quantum systems, *Quant. Semiclass. Opt.: J. Eur. Opt. Soc. B* **8**, 1103 (1996).
 - [21] J. Gambetta and H. M. Wiseman, State and dynamical parameter estimation for open quantum systems, *Phys. Rev. A* **64**, 042105 (2001).
 - [22] M. Tsang, Continuous Quantum Hypothesis Testing, *Phys. Rev. Lett.* **108**, 170502 (2012).
 - [23] S. Gammelmark and K. Mølmer, Bayesian parameter inference from continuously monitored quantum systems, *Phys. Rev. A* **87**, 032115 (2013).
 - [24] A. H. Kiilerich and K. Mølmer, Estimation of atomic interaction parameters by photon counting, *Phys. Rev. A* **89**, 052110 (2014).
 - [25] A. H. Kiilerich and K. Mølmer, Parameter estimation by multichannel photon counting, *Phys. Rev. A* **91**, 012119 (2015).
 - [26] A. H. Kiilerich and K. Mølmer, Bayesian parameter estimation by continuous homodyne detection, *Phys. Rev. A* **94**, 032103 (2016).
 - [27] A. H. Kiilerich and K. Mølmer, Random search for a dark resonance, *Phys. Rev. A* **95**, 022110 (2017).
 - [28] P. Haikka, Y. Kubo, A. Bienfait, P. Bertet, and K. Mølmer, Proposal for detecting a single electron spin in a microwave resonator, *Phys. Rev. A* **95**, 022306 (2017).
 - [29] A. H. Kiilerich and K. Mølmer, Hypothesis testing with a continuously monitored quantum system, [arXiv:1804.08900](https://arxiv.org/abs/1804.08900).
 - [30] S. Gammelmark and K. Mølmer, Fisher Information and the Quantum Cramér-Rao Sensitivity Limit of Continuous Measurements, *Phys. Rev. Lett.* **112**, 170401 (2014).
 - [31] M. Guță, Fisher information and asymptotic normality in system identification for quantum Markov chains, *Phys. Rev. A* **83**, 062324 (2011).
 - [32] H.-P. Breuer and F. Petruccione, *The Theory of Open Quantum Systems* (Oxford University Press on Demand, Oxford, 2002).

- [33] N. Ohlsson, R. K. Mohan, and S. Kröll, Quantum computer hardware based on rare-earth-ion-doped inorganic crystals, *Opt. Commun.* **201**, 71 (2002).
- [34] J. H. Wesenberg, K. Mølmer, L. Rippe, and S. Kröll, Scalable designs for quantum computing with rare-earth-ion-doped crystals, *Phys. Rev. A* **75**, 012304 (2007).
- [35] J. D. Jackson, *Classical Electrodynamics* (John Wiley & Sons, New York, 2007).
- [36] F. R. Graf, A. Renn, U. P. Wild, and M. Mitsunaga, Site interference in Stark-modulated photon echoes, *Phys. Rev. B* **55**, 11225 (1997).
- [37] R. L. Ahlefeldt, W. D. Hutchison, and M. J. Sellars, Characterisation of $\text{EuCl}_3 \cdot 6\text{H}_2\text{O}$ for multi-qubit quantum processing, in *Quantum Electronics Conference & Lasers and Electro-Optics (CLEO/IQEC/PACIFIC RIM), 2011* (IEEE, New York, 2011), pp. 1791–1793.
- [38] D. Jaksch, J. I. Cirac, P. Zoller, S. L. Rolston, R. Côté, and M. D. Lukin, Fast Quantum Gates for Neutral Atoms, *Phys. Rev. Lett.* **85**, 2208 (2000).
- [39] L. Childress, M. V. Gurudev Dutt, J. M. Taylor, A. S. Zibrov, F. Jelezko, J. Wrachtrup, P. R. Hemmer, and M. D. Lukin, Coherent dynamics of coupled electron and nuclear spin qubits in diamond, *Science* **314**, 281 (2006).
- [40] J. R. Maze, J. M. Taylor, and M. D. Lukin, Electron spin decoherence of single nitrogen-vacancy defects in diamond, *Phys. Rev. B* **78**, 094303 (2008).
- [41] T. H. Taminiau, J. J. T. Wagenaar, T. van der Sar, F. Jelezko, V. V. Dobrovitski, and R. Hanson, Detection and Control of Individual Nuclear Spins using a Weakly Coupled Electron Spin, *Phys. Rev. Lett.* **109**, 137602 (2012).
- [42] N. Zhao, J. Honert, B. Schmid, M. Klas, J. Isoya, M. Markham, D. Twitchen, F. Jelezko, R.-B. Liu, H. Fedder *et al.*, Sensing single remote nuclear spins, *Nat. Nanotechnol.* **7**, 657 (2012).